Nanoscale

ROYAL SOCIETY OF CHEMISTRY

PAPER

View Article Online
View Journal | View Issue

Cite this: *Nanoscale*, 2025, **17**, 1980

Face-controlled chirality induction in octahedral thiacalixarene-based porous coordination cages†

Ivan V. Khariushin,[a] Alexander S. Ovsyannikov,[b] Stéphane A. Baudron,[a] Jas S. Ward,[c] Anniina Kiesilä,[c] Kari Rissanen,[c] Elina Kalenius,[c] Matthieu Chessé,[d] Beata Nowicka,[e] Svetlana E. Solovieva,[f] Igor S. Antipin,[f] Véronique Bulach[a] and Sylvie Ferlay *[a]

Received 4th September 2024,
Accepted 26th November 2024

DOI: 10.1039/d4nr03622k

rsc.li/nanoscale

Nanosized chiral octahedral M_{32} coordination cages were prepared *via* self-assembly of sulfonylcalix[4]arene tetranuclear M(II) clusters (M = Co or Ni) with enantiomerically enriched linkers based on tris(dipyrrinato)cobalt(III) complexes, appended with peripheral carboxylic groups. Two pairs of enantiomers of cages were obtained and unambiguously characterized from a structural point of view, using single crystal X-ray diffraction. Chiral-HPLC was used to evidence the enantiomers. In the solid state, the compounds present intrinsic and extrinsic porosity: the intrinsic porosity is linked with the size of the cages, which present an inner diameter of *ca.* 19 Å. The obtained solid-state supramolecular architectures demonstrated good performances as adsorbents for water and 2-butanol guest molecules.

Introduction

Permanently nanoporous molecular coordination cages (containers or capsules) and metal–organic cages (MOCs) or polyhedra (polygons) (MOPs)[1–6] belong to the well-known class of supramolecular cages that have attracted much attention over the last few decades. Owing to their nanosize and stability, these compounds present porosity in the solid state due to the presence of an internal cavity inherent to their molecular nature, and also the additional extrinsic porosity resulting from the specific packing of molecules in the crystal.[7] The applications of such porous symmetrical entities cover fields such as host/guest chemistry,[8] molecular separation/storage,[9,10] sensing,[11] catalysis,[12–14] drug delivery[15] and biomedical applications.[16,17] These compounds have been often compared to their analogues metal–organic frameworks (MOFs), but they present the advantage of being soluble, which simplifies their purification and use.

Thanks to infinite synthetic possibilities, a large variety of MOCs have been reported, although their formation mainly results from self-assembly of one type of ligand and metal ion.[18,19] The use of components being able to display some specific intermolecular interactions with guest molecules and the understanding of their assembly are key parameters for the control and the optimization of the porosity and the selectivity of these molecular compounds.

In this context, it is all the more interesting to use intrinsically porous starting components. Cavity-shaped calixarenes are thus good candidates to build nanosized highly porous compounds. Thiacalix[4]arene[20] (H_4TCA) and its oxidized analogue sulfonylcalix[4]arene[21] (H_4SO_2TCA) in cone conformation (Fig. 1a) are attractive building blocks, presenting a hydrophobic cavity. As classical calix[4]arenes,[22,23] they have demonstrated a fascinating ability of selective trapping different small organic molecules or gases.[24–26] When combined with divalent metal ions, these building blocks can lead to the formation of nanosized MOCs. The first porous coordination cage based on the macrocyclic thiacalixarene was reported in 2012.[27] Several coordination cages based on thiacalixarenes have since been reported:[28,29] coordination clus-

---

[a] *Université de Strasbourg, CNRS, CMC UMR 7140, F-67000 Strasbourg, France. E-mail: ferlay@unistra.fr*

[b] *Arbuzov Institute of Organic and Physical Chemistry, FRC Kazan Scientific Center, Russian Academy of Sciences, Arbuzova 8, Kazan 420088, Russian Federation*

[c] *University of Jyvaskyla, Department of Chemistry, 40014 Jyväskylä, Finland*

[d] *LIMA UMR 7042, Université de Strasbourg et CNRS et UHA, European School of Chemistry, Polymers and Materials (ECPM), 25 Rue Becquerel, F-67087 Strasbourg, France*

[e] *Faculty of Chemistry, Jagiellonian University, Gronostajowa 2, 30-387 Kraków, Poland*

[f] *Kazan Federal University, Kremlevskaya 18, Kazan 420008, Russian Federation*

† Electronic supplementary information (ESI) available: The asymmetric units for $\mathbf{[M_4SO_2TCA(\mu_4\text{-}OH_2)]_6[\Delta/\Lambda\text{-}Co(L)_3]_8}$ (M = Ni or Co), chiral HPLC chromatograms for $\mathbf{\Delta/\Lambda\text{-}Co(HL)_3}$ and $\mathbf{[M_4SO_2TCA(\mu_4\text{-}OH_2)]_6[\Delta/\Lambda\text{-}Co(L)_3]_8}$ (M = Ni or Co), CD spectra for $\mathbf{[Co_4SO_2TCA(\mu_4\text{-}OH_2)]_6[\Lambda/\Delta\text{-}Co(L)_3]_8}$, XRPD and ESI-MS for $\mathbf{[M_4SO_2TCA(\mu_4\text{-}OH_2)]_6[\Delta/\Lambda\text{-}Co(L)_3]_8}$ (M = Ni or Co), IM-MS details of calculations for $\mathbf{[M_4SO_2TCA(\mu_4\text{-}OH_2)]_6[\Delta/\Lambda\text{-}Co(L)_3]_8}$ (M = Ni or Co) and isotherms of water and rac-2-butanol and S-2 butanol adsorption for $\mathbf{[M_4SO_2TCA(\mu_4\text{-}OH_2)]_6[\Delta,\Lambda\text{-}Co(L)_3]_8}$ (M = Ni or Co). CCDC 2374315, 2374330, 2374431 and 2374432. For ESI and crystallographic data in CIF or other electronic format see DOI: **https://doi.org/10.1039/d4nr03622k**

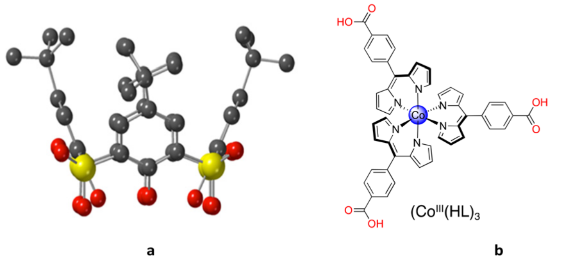

Fig. 1 (a) Tetrasulfonylcalix[4]arene ($H_4SO_2TCA^{4-}$) in cone conformation and (b) the tris(dipyrrinatocarboxylic)-cobalt(III) complex (**Co^{III}(HL)$_3$**) as building blocks for the formation of nanosized cages.

ters,[30] capsules or (super)containers,[31,32] and cages,[27,33] leading, as we recently reviewed, to polyhedra displaying a large variety of adaptable geometries.[34] The strategy to form MOCs using H_4TCA or H_4SO_2TCA is generally based on the combination of *in situ* generated “shuttlecock-like” $[M^{II}_4(\mu_4\text{-}H_2O)TCA]^{4+}$ (or $[M^{II}_4(\mu_4\text{-}H_2O)SO_2TCA]^{4+}$) building blocks, acting as *tetrakis*-connecting nodes, with negatively charged polytopic carboxylate ligands.[35] This approach has been efficiently exploited for the design of new thiacalixarene-based MOCs, exhibiting different smart properties. Among them, chiral thiacalixarene-based MOCs, demonstrating homochirality,[36,37] are of particular interest: for example, using the salen metalloligands incorporating stereogenic centres on the organic backbone, octahedral homochiral thiacalixarene cages are formed, in which exciting regio- and enantioselective photodimerization was demonstrated.[38]

Chiral MOCs[39,40] may find applications in the fields of chiral memory,[41] stereochemical communication,[42] enantioselective recognition and separation[43] or enantiomeric catalysis.[38,44,45] The formation of chiral polyhedral MOCs results, in most of the cases, from the introduction of stereogenic centres into the polyhedral entities to remove inversion centres and mirror planes inherent to symmetrical cages.

Recently, we designed octahedral MOCs, resulting from the linkage of tetranuclear nickel(II) or cobalt(II) clusters supported by sulfonylcalix[4]arene by using the racemic tris(dipyrrinato) cobalt(III) complex **[*rac*-Co(L)$_3$]** (Fig. 1b), appended with peripheral carboxylic acid groups, which were successfully used for methane separation from C_2-hydrocarbons.[46] Taking into account that such kinds of chelated metalloligands can exist in two enantiomeric forms (Δ or Λ), it can be assumed that the use of enantiopure triangular linkers can afford the formation of face-directed octahedron shaped thiacalixarene-based cages, displaying homochirality. The use of a metalloligand, where the stereogenic center is the metal complex, has been scarcely reported in the literature until now for the formation of coordination cages,[47,48] and, to the best of our knowledge, not with thiacalixarene-based cages.

In this work, we report on the first example of sulfonylcalix[4]arene-based octahedral MOCs, displaying face-controlled chirality induction, due to insertion of an enantiopure metallocenter, based on the tris(dipyrrinato)cobalt(III) complex with the peripheral carboxylic acid groups **[Δ-Co(L)$_3$]** and **[Λ-Co(L)$_3$]** (Fig. 1b). A series of four enantiomerically pure porous coordination compounds have been synthesized and characterized. The preliminary adsorption properties towards chiral guests were studied.

Results and discussion

Formation of enantiomerically pure connectors

In order to obtain the enantiopure tris(dipyrrinato)cobalt(III) precursors, an adaptation of the method described by Wuest *et al.*,[49] and based on the interaction with the chiral reaction partner (−)-cinchonidine followed by separation of formed diastereomers by dissolving in THF and column chromatography under acidic conditions, was successfully applied to isolate **Λ-Co(HL)$_3$** and **Δ-Co(HL)$_3$** (see the Experimental section; see also Fig. 3a). The enantiomeric enrichment of the complexes was confirmed by circular dichroism (CD) as presented in Fig. 2. In addition, chiral HPLC demonstrated a retention time of 16.70 min for **Λ-Co(HL)$_3$** and 14.87 min for **Δ-Co(HL)$_3$**. According to the integration of peaks, the value of ee was estimated to be 92% for **Λ-Co(HL)$_3$** and 85% for **Δ-Co(HL)$_3$** (Fig. S1 in the ESI†).

These data suggested that the compounds are enantiomerically enriched. The fact that they are stable in a THF solution and also in the solid state allows them to be used for the formation of cages.

Formation and characterization of homochiral octahedral M_{32} cages

Using the same conditions as previously described,[46] a one-pot three-component reaction for obtaining octahedral cages was performed with a 4 : 3 : 12 mixture of **Λ/Δ-Co(HL)$_3$**, H_4SO_2TCA, and $MCl_2\cdot 6H_2O$ (M = Co or Ni) with Et_3N (30 eq.) in a 1/1 *N*,*N*-dimethylformamide (DMF) and MeOH mixture (see the Experimental section). The slow diffusion technique (see the

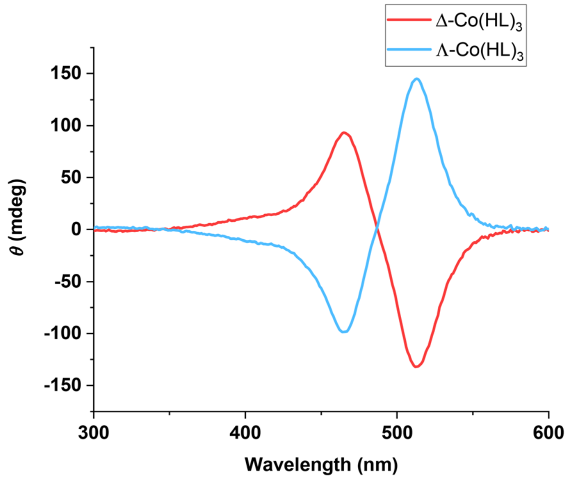

Fig. 2 CD spectra of **Λ-Co(HL)$_3$** and **Δ-Co(HL)$_3$** (RT, 5 × 10^{-5} M, THF, 2 mm).

Experimental section) at RT led to red single crystals in 53–78% yields. The crystals are soluble in dichloromethane (DCM). Two series of enantiomers were obtained, and they were all characterised first using single-crystal X-ray diffraction (SCXRD). The four compounds are isomorphous and crystallize in the non-centrosymmetric *R*32 trigonal space group (see the crystallographic table, Table 1) and the asymmetric unit is shown in Fig. S2 in the ESI,† for each compound. The four compounds are represented by one of the two following general formulae: $[\mathbf{M^{II}{}_4SO_2TCA(\mu_4\text{-}OH_2)}]_6[\mathbf{\Lambda\text{-}Co^{III}(L)_3}]_8\cdot \boldsymbol{n}\mathbf{DMF}\cdot\boldsymbol{m}\mathbf{H_2O}$ or $[\mathbf{M^{II}{}_4SO_2TCA(\mu_4\text{-}OH_2)}]_6[\mathbf{\Delta\text{-}Co^{III}(L)_3}]_8\cdot \boldsymbol{n}\mathbf{DMF}\cdot\boldsymbol{m}\mathbf{H_2O}$ (M = Co or Ni). The cages are formed from six $[\mathbf{1}\text{-}M^{II}_4(\mu_4\text{-}H_2O)]^{4+}$ "shuttlecock-like" units, forming the vertices of the octahedron, and eight enantiomerically pure $\mathbf{\Lambda/\Delta\text{-}Co(HL)_3}^{3-}$ units (see Fig. 3a), forming the eight faces of the octahedron, and thus each connecting three vertices (Fig. 3b). The characteristic distances of the species are shown in Table 2. The distances within the cages will not be further discussed here. The dimensions of the nanosized cages are approximately 46.5 × 46.5 × 46.5 Å^3 and the inner cavity has a diameter of *ca.* 19 Å.

Disorder is observed in the N6 environment around the cobalt(III) cations of the $(Co^{III}L_3)^{3-}$ carboxylate connectors. The Flack parameters were refined for the four compounds (see the crystallographic table, Table 1), but were found to deviate too much from zero to be relied upon; therefore the absolute configurations assigned were based on the presence of unchanging chiral centres used in the syntheses. The inability to correctly refine the Flack parameters in all structures can be attributed to the large amount of electron density belonging to disordered solvent molecules (calculated porosity >70%) that was accounted for using SQUEEZE within PLATON.[50]

For the 4 compounds, when analyzed in their mother liquor, well-defined powder XRD patterns could be observed (see Fig. S3 in the ESI†), demonstrating their perfect isostructurality, but slightly deviating from the corresponding calculated diagram, due to the dynamic presence of a high number of solvent molecules in the unit cell, which causes some reorganization of the position of the cages in the unit cell. When exposed to air, the PXRD patterns of the four powdered compounds indicate amorphization, as previously observed for the

Table 1 Crystallographic data for $[M_4SO_2TCA(\mu_4\text{-}OH_2)]_6[\Delta/\Lambda\text{-}Co(L)_3]$ (M = Co or Ni), recorded at *T* = 120 K

Compound	$[\mathbf{Co_4SO_2TCA}]_6[\mathbf{\Lambda\text{-}Co(L)_3}]_8$	$[\mathbf{Co_4SO_2TCA}]_6[\mathbf{\Delta\text{-}Co(L)_3}]_8$	$[\mathbf{Ni_4SO_2TCA}]_6[\mathbf{\Lambda\text{-}Co(L)_3}]_8$	$[\mathbf{Ni_4SO_2TCA}]_6[\mathbf{\Delta\text{-}Co(L)_3}]_8$
Formula[a]	$C_{624}H_{504}Co_{32}N_{48}O_{126}S_{24}$	$C_{624}H_{504}Co_{32}N_{48}O_{126}S_{24}$	$C_{624}H_{504}Co_8N_{48}Ni_{24}O_{126}S_{24}$	$C_{624}H_{504}Co_8N_{48}Ni_{24}O_{126}S_{24}$
Formula weight (g mol^{-1})	13 346.06	13 346.06	13 340.78	13 340.78
Colour & habit	Red block	Red block	Red block	Red block
Crystal dimensions (mm)	0.30 × 0.34 × 0.43	0.24 × 0.34 × 0.38	0.27 × 0.30 × 0.35	0.21 × 0.32 × 0.45
Crystal system	Trigonal	Trigonal	Trigonal	Trigonal
Space group	*R*32	*R*32	*R*32	*R*32
a (Å)	37.0736(6)	37.9778(10)	37.0388(3)	36.9578(6)
b (Å)	37.0736(6)	37.9778(10)	37.0388(3)	36.9578(6)
c (Å)	190.622(3)	190.170(4)	190.1726(19)	190.122(2)
α (°)	90	90	90	90
β (°)	90	90	90	90
γ (°)	120	120	120	120
V (Å)	226 898(8)	237 538(13)	225 939(5)	224 892(8)
Z	6	6	6	6
$\rho_{\text{calc.}}$ (g cm^3)	0.586	0.560	0.588	0.591
F(000)	41 040	41 040	41 184	44 312
μ (mm^{-1})	3.245	3.100	1.561	1.568
Temperature (K)	120.0(1)	120.0(1)	120.0(1)	120.0(1)
$\theta_{\max}$ [°]	61.2	51.3	61.2	61.2
Total reflections	331 644	298 743	290 455	309 391
Independent reflections	77 167	57 138	77 139	76 366
Reflections ($I_o > 2\sigma[I_o]$)	33 790	34 910	49 201	48 433
R_{int}	0.159	0.101	0.102	0.066
Parameters	2296	2257	2274	2270
Restraints	321	294	384	109
GooF (F^2)	0.892	0.985	0.923	1.023
R_1 ($I_o > 2\sigma[I_o]$)	0.0830	0.0873	0.0554	0.0549
R_1 (all reflections)	0.1476	0.1282	0.0848	0.0861
wR_2 ($I_o > 2\sigma[I_o]$)	0.2070	0.2420	0.1319	0.1495
wR_2 (all reflections)	0.2531	0.2756	0.1492	0.1680
Largest peak (e Å^{-3})	0.568	0.517	0.513	0.424
Largest hole (e Å^{-3})	−0.526	−0.564	−0.447	−0.451
Flack parameter[b]	0.422(4)	0.242(5)	0.215(5)	0.181(4)
CCDC	2374431	2374315	2374432	2374330

[a] SQUEEZE[50] within PLATON was used to account for the large amount of heavily disordered solvates within the cavities of the compounds. No adjustments were made (formula, formula weight, density, *etc.*) to account for the use of SQUEEZE. [b] All compounds were refined as 2-component inversion twins, as the use of PLATON SQUEEZE resulted in ambiguous values for the Flack parameters. As a consequence, the reported Flack parameters can be ignored and are only reported herein for completeness. The assignment of stereocentres were made based on the use of unchanging chiral centres in the synthetic precursors.

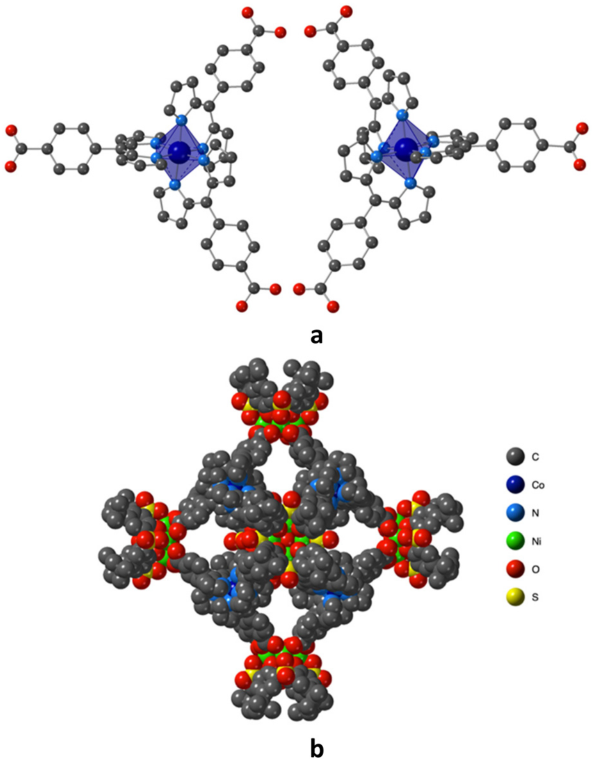

Fig. 3 XRD analysis of the formed $[M_4SO_2TCA(\mu_4\text{-}OH_2)]_6[\Delta/\Lambda\text{-}Co(L)_3]_8 \cdot n\mathrm{DMF} \cdot m\mathrm{H_2O}$: (a) enantiomerically pure $\Lambda/\Delta\text{-}Co(L)_3^{3-}$ components and (b) representation of the formed cages.

racemic parent compound,[46] and more generally for large coordination porous species.[38]

The crystalline compounds were also characterized by a variety of techniques including CD, ESI-MS, ion mobility mass spectrometry (IM-MS), and chiral HPLC.

The ESI-MS data (Fig. S4 in the ESI†) demonstrated the abundant formation of dipyrrin-based MOCs at the *m*/*z* range of 2220–2230, which corresponds to intact MOCs on the 6^- charge state with some $n\mathrm{H_2O}/m\mathrm{DMF}$ adduct formation, which is common for such types of materials. The 6^- charge state can be related to the deprotonation of $\mu_4\text{-}OH_2$ in each shuttlecock moiety.

In addition to ESI-MS, IM-MS measurements were performed. $^{\mathrm{DT}}\mathrm{CCS}_{\mathrm{N_2}}$ values were obtained, ranging from 1830.0 to 1846.1 Å^2, in agreement with the values calculated from the single-crystal XRD structure: 1862.72 Å^2 (see calculations in the ESI†).

The obtained ESI-MS and IM-MS data account for the formation of the nanosized species. It is worth mentioning that the obtained MS data are also strong evidence of the high stability of MOCs in solution.

The CD spectra of the chiral cages **$[Ni_4SO_2TCA(\mu_4\text{-}OH_2)]_6[\Lambda\text{-}Co(L)_3]_8$** and **$[Ni_4SO_2TCA(\mu_4\text{-}OH_2)]_6[\Delta\text{-}Co(L)_3]_8$** in DCM solution show curves with peaks at 515 nm and 465 nm, which are almost perfect mirror images providing evidence, in both cases, of a high enantiomeric excess (ee) (Fig. 4, and Fig. S5 in the ESI† for **$[Co_4SO_2TCA(\mu_4\text{-}OH_2)]_6[\Delta/\Lambda\text{-}Co(L)_3]$**). The obtained values of ellipticity are 421.29 and −479.56 mdeg for **$[Ni_4SO_2TCA(\mu_4\text{-}OH_2)]_6[\Lambda\text{-}Co(L)_3]_8$** and 395.16 and 452.06 mdeg for **$[Ni_4SO_2TCA(\mu_4\text{-}OH_2)]_6[\Delta\text{-}Co(L)_3]_8$**, which are much larger than the ones observed for the connectors: **$\Lambda\text{-}Co(HL)_3$** (−98.47 and 144.44 mdeg) and **$\Delta\text{-}Co(HL)_3$** (91.9 and −131.7 mdeg). This confirms their presence in a large species.

The strong evidence regarding the large ee for **$[Co_4SO_2TCA(\mu_4\text{-}OH_2)]_6[\Delta/\Lambda\text{-}Co(L)_3]$** and **$[Ni_4SO_2TCA(\mu_4\text{-}OH_2)]_6[\Delta/\Lambda\text{-}Co(L)_3]$** cages was provided using chiral HPLC experiments. The chiral HPLC experiments demonstrated the formation of chiral MOCs with ee up to 97%. The data of the HPLC experiments are summarized in Table 3 and are presented in Fig. S6 in the ESI.†

Sorption properties of octahedral M_{32} cages in the solid state

Gas adsorption of some calixarene-based MOCs has been recently reviewed.[51] However, there are only a few reports on vapor sorption by MOCs. They include water sorption studies in polyoxometalate-based cages,[52] as well as very interesting reports on fluorescence switchability by $CHCl_3$ vapor sorption[53] or colour change induced by ammonia vapor intake[54] in tetrahedral MOCs.

The sorption properties of the four MOCs have been investigated by the gravimetric dynamic vapor sorption method. Freshly filtered-off samples were desolvated under dry N_2 flow with a stepwise increase in temperature from 25 to 120 °C. The initial decrease in mass is very fast (Fig. S7 in the ESI†), indicating that the release of solvents from crystallization (DMF and MeOH) starts at room temperature immediately upon removal from the mother liquor, for **$[Co_4SO_2TCA(\mu_4\text{-}OH_2)]_6[\Lambda\text{-}Co(L)_3]_8$**. For all samples, the registered mass loss of about 48% corresponds roughly to the release of 166 DMF molecules per formula unit (one cage).

The water sorption isotherms, for the four compounds, show almost linear change of mass with increasing relative humidity (RH) and narrow hysteresis (Fig. 5). At 90% RH, the amount of adsorbed water reaches only 10–12%, which corres-

Table 2 Characteristic distances around the metal ions in the structure of MOCs based on the chiral dipyrrin connectors **$\Delta\text{-}Co(HL)_3$** and **$\Lambda\text{-}Co(HL)_3$**

$[M_4SO_2TCA(\mu_4\text{-}OH_2)]_6[\Delta,\Lambda\text{-}Co(L)_3]_8 \cdot n\mathrm{DMF} \cdot m\mathrm{H_2O}$ (M = Co^{II} or Ni^{II})

	$M\text{–}O_{(H_2O)}$, Å	M–M, Å	Co–N, Å
$[Co_4SO_2TCA]_6[\Lambda\text{-}Co(L)_3]_8$	2.196(9)–2.267(9)	2.988(4)–3.027(3)	1.857(14)–1.954(14)
$[Co_4SO_2TCA]_6[\Delta\text{-}Co(L)_3]_8$	2.114(10)–2.304(9)	2.970(5)–3.030(3)	1.860(9)–1.970(9)
$[Ni_4SO_2TCA]_6[\Lambda\text{-}Co(L)_3]_8$	2.149(5)–2.235(5)	2.957(2)–2.994(2)	1.880(5)–1.950(5)
$[Ni_4SO_2TCA]_6[\Delta\text{-}Co(L)_3]_8$	2.160(5)–2.215(6)	2.944(2)–2.983(3)	1.883(8)–1.949(5)

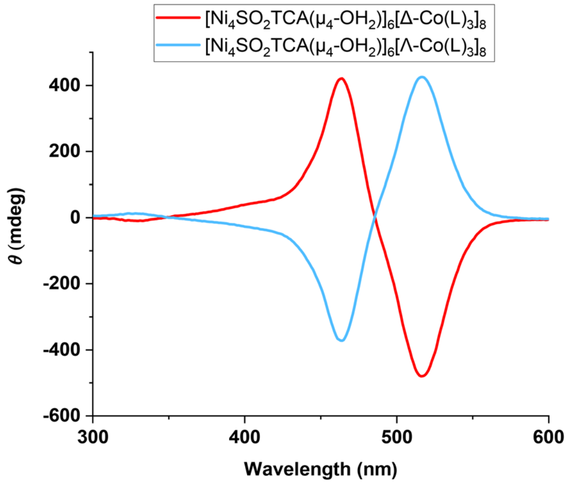

Fig. 4 CD spectra of $[Ni_4SO_2TCA(\mu_4\text{-}OH_2)]_6[\Lambda\text{-}Co(L)_3]_8$ and $[Ni_4SO_2TCA(\mu_4\text{-}OH_2)]_6[\Delta\text{-}Co(L)_3]_8$ (RT, 5×10^{-5} M, DCM, cuvette length = 2 mm).

Table 3 For MOCs based on the chiral dipyrrin connectors $\Delta\text{-}Co(HL)_3$ and $\Lambda\text{-}Co(HL)_3$: the retention time and ee using chiral HPLC

	Retention time, min	ee, %
$[Co_4SO_2TCA(\mu_4\text{-}OH_2)]_6[\Lambda\text{-}Co(L)_3]_8$	51.05	97
$[Co_4SO_2TCA(\mu_4\text{-}OH_2)]_6[\Delta\text{-}Co(L)_3]_8$	28.10	96
$[Ni_4SO_2TCA(\mu_4\text{-}OH_2)]_6[\Lambda\text{-}Co(L)_3]_8$	51.06	95
$[Ni_4SO_2TCA(\mu_4\text{-}OH_2)]_6[\Delta\text{-}Co(L)_3]_8$	28.14	92

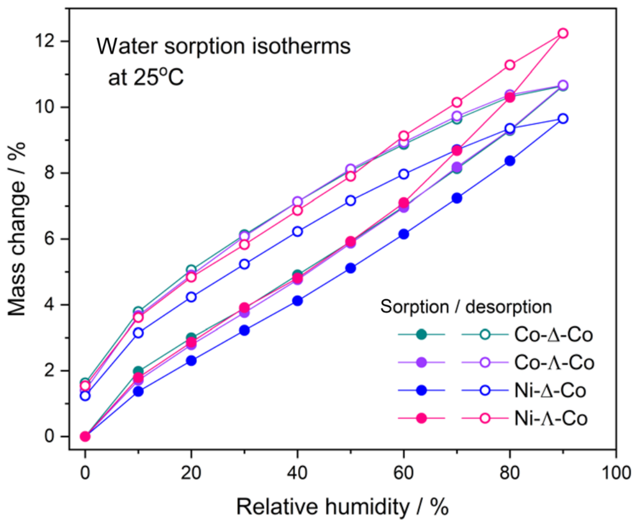

Fig. 5 Water sorption isotherms at 25 °C for $[M_4SO_2TCA(\mu_4\text{-}OH_2)]_6[\Delta/\Lambda\text{-}Co(L)_3]$.

ponds to about 80 H_2O molecules. We assume that the adsorbed water molecules are located mostly around the eight shuttlecock moieties, where the sulfonyl and carboxylic groups facilitate the formation of hydrogen bonds. The small mass increase indicates that water does not fill the full volume of the cage, most probably due to its large size and mostly hydrophobic inner surface formed by phenylene and pyrrolyl rings. After the desorption process, about 12 water molecules (1.6%) are retained. In the second sorption cycle, the same maximum amount of water is reached and the hysteresis becomes even narrower (Fig. S8 in the ESI†). After water sorption, the samples can be reactivated at 120 °C to regain the original sorption capacity. The small differences between the four compounds (slightly lower sorption for $[Ni_4SO_2TCA(\mu_4\text{-}OH_2)]_6[\Lambda\text{-}Co(L)_3]_8$ and increase in sorption at high RH for $[Ni_4SO_2TCA(\mu_4\text{-}OH_2)]_6[\Lambda\text{-}Co(L)_3]_8$) may be related to the different sizes of crystallites.

The sorption of 2-butanol was studied in order to evaluate the potential of the cages in enantioselective sorption. Initial experiments were conducted on the racemic mixture. In contrast to water sorption, the compounds show a sharp initial intake of 2-butanol (over 10% mass increase at 5% p/p_0), consistent with their porous characteristic (Fig. 6). Then the mass increase is almost linear and reaches about 42%, which corresponds to an intake of 76 molecules per formula unit. More effective sorption of 2-butanol than that of water may be connected with its lower polarity and larger size, which facilitate trapping within the cages. However, the adsorbed amount of 2-butanol is much too small to fill the voids in the structure originally occupied by the crystallization solvent, which corroborates the supposed collapse of the crystal lattice upon desolvation. Like in the case of water, some 2-butanol is retained after desorption (10–16 molecules), and in the subsequent sorption cycles (Fig. S9 in the ESI†), the sorption hysteresis becomes narrower. The retained 2-butanol can be removed by activation at 120 °C. There are some small differences in the adsorbed amount of 2-butanol between the compounds. Like in the case of adsorption of water, $[Ni_4SO_2TCA(\mu_4\text{-}OH_2)]_6[\Lambda\text{-}Co(L)_3]_8$ shows the highest intake and $[Ni_4SO_2TCA(\mu_4\text{-}OH_2)]_6[\Lambda\text{-}$

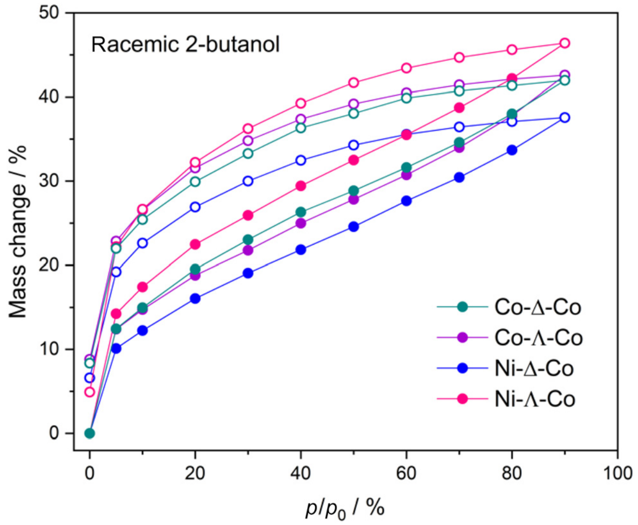

Fig. 6 Racemic 2-butanol sorption isotherms at 25 °C for $[M_4SO_2TCA(\mu_4\text{-}OH_2)]_6[\Delta/\Lambda\text{-}Co(L)_3]$; full circles – sorption, empty circles – desorption.

$Co(L)_3]_8$ shows the lowest intake. However, we also observed some variations in sorption between different batches of the same compound. They included varied sorption kinetics (time to achieve equilibrium in each step) and the maximum mass increase differing up to 2%. This behaviour confirms our hypothesis that the differences in sorption characteristics are connected with the crystal size and the extent of their collapse upon the loss of crystallization solvent. The dependence of gas or vapor sorption properties on the post-synthetic treatment, including contact with water or organic solvents, was also observed in other MOC structures.[55,56]

In order to check whether there is a preferential sorption of one enantiomer, we performed analogous sorption studies using enantiopure *S*-2-butanol. The resulting isotherms (Fig. S10 in the ESI†) practically coincide with those of racemic 2-butanol within the observed differences described above. Therefore, we may conclude that the cages, despite their chirality, do not show enantioselectivity towards 2-butanol. Successful separation of 2-butanol enantiomers was found for some chiral 2D and 3D MOFs.[57–59] In all these cases, the size of the voids in the porous MOF structures is much smaller than the dimensions of the inner cavity of the **$[M_4SO_2TCA(\mu_4\text{-}OH_2)]_6[\Delta/\Lambda\text{-}Co(L)_3]_8$** cages. Therefore, we believe that the lack of enantioselectivity is caused by the fact that 2-butanol molecules can adopt different conformations inside the large cages without direct interactions with the cage chiral skeleton.

Experimental

Synthesis

General. All reagents and solvents were of analytical grade and purchased from commercial sources and were used without further purification. The syntheses of (H_4SO_2TCA)[60] and the racemic ***rac*-$Co(HL_1)_3$** (L = 5-(4-carboxyl-phenyl)-4,6-dipyrrinato) were performed as previously described.[61,62] The separation of ***rac*-$Co(HL_1)_3$** is adapted from a previously reported procedure.[49]

Chiral separation for Λ/Δ-$Co(HL)_3$. Tris[5-(4-carboxyphenyl)-4,6-dipyrrinato] Co(III) (***rac*-$Co(HL_1)_3$**) (0.350 g, 0.4 mmol) and (−)-cinchonidine (0.2425 g, 0.8 mmol) were dissolved in 20 mL of THF. The reaction mixture was refluxed overnight, then cooled in a fridge, filtered off and washed one time with cold THF to afford a red solid (Λ) and a red filtrate (Δ).

Both compounds display the same NMR data; below is the numbering scheme used for NMR data.

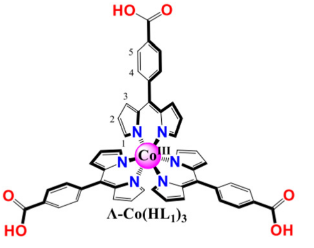
Λ-$Co(HL_1)_3$

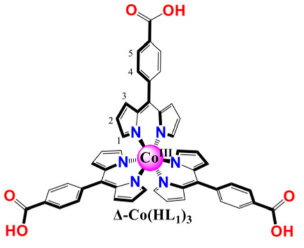
Δ-$Co(HL_1)_3$

^{1}H-NMR (DMSO-d_6, 500 MHz, 25 °C) δ ppm: 8.08 (d, *J* = 7.8 Hz, 6H, H^5), 7.56 (d, *J* = 7.8 Hz, 6H, H^4), 6.64 (m, 6H, H^3), 6.45 (m, 6H, H^1), 6.35 (m, 6H, H^2).

Λ-Tris[5-(4-carboxyphenyl)-4,6-dipyrrinato] Co(III) (***Λ-$Co(HL)_3$***). The red solid was dissolved in a mixture of ethyl acetate/trifluoroacetic acid (EA/TFA = 100/0.3) and then purified by column chromatography (SiO_2, eluent – EA/TFA = 100/0.3); it afforded a bright red solid (77%, 0.135 g).

CD (5×10^{-5} M, THF, 2 mm): 465 nm (θ = −98.47 mdeg), 515 nm (θ = 144.44 mdeg).

Chiral HPLC (ChiralPak IA, hexane/THF/TFA = 80/20/0.1, flow rate = 0.8 mL min^{-1}, λ = 470 nm, 25 °C): 16.70 min, ee = 92%.

Δ-Tris[5-(4-carboxyphenyl)-4,6-dipyrrinato] Co(III) (***Δ-$Co(HL)_3$***). The obtained filtrate was evaporated and the dark red residue was dissolved in the mixture EA/TFA = 100/0.3 and then purified by column chromatography (SiO_2, eluent – EA/TFA = 100/0.3); it afforded a bright red solid (63%, 0.111 g).

CD (5×10^{-5} M, THF, 2 mm): 465 nm (θ = 91.9 mdeg), 515 nm (θ = −131.7 mdeg).

Chiral HPLC (ChiralPak IA, hexane/THF/TFA = 80/20/0.1, flow rate = 0.8 mL min^{-1}, λ = 470 nm, 25 °C): 14.87 min, ee = 85%.

Crystallisation for $[M_4SO_2TCA(\mu_4\text{-}OH_2)]_6[\Lambda/\Delta\text{-}Co(L)_3]_8$ (M = Ni or Co). The same procedure was applied for the four compounds.

(**Λ/Δ-$Co(HL_1)_3$**) (0.03 g, 0.03 mmol), sulfonylcalix[4]arene (0.02 g, 0.02 mmol) and cobalt(II) chloride hexahydrate (0.022 g, 0.094 mmol) were dissolved in 5 mL of DMF and then were placed in a tube. A mixture of 1 mL of MeOH and 1 mL of DMF was placed in the tube above the DMF solution. Triethylamine (0.03 mL, 0.23 mmol) was dissolved in 3 mL of MeOH and the triethylamine solution was placed in the tube above the mixture of DMF and MeOH. The tube was sealed and left for two weeks. Octahedral red crystals suitable for further analysis were collected *via* filtration.

$[Co_4SO_2TCA(\mu_4\text{-}OH_2)]_6[\Delta\text{-}Co(L)_3]_8$. Yield = 55%.

ESI-MS: calculated *m*/*z* for $[M + H_2O - 6H]^{6-}$ 2226.3, *m*/*z* found 2224.4.

IM-MS: found $^{DT}CCS_{N_2}$ = 1833.6 Å^2.

Elemental analysis ($C_{624}H_{504}Co_{32}N_{48}O_{126}S_{24}\cdot 40DMF\cdot 22H_2O$): % calculated: C, 53.62%; H, 5.01%; N, 7.40%; % found: C, 53.62%; H, 5.01%; N, 7.37%.

CD (5×10^{-5} M, DCM, 2 mm): 467 nm (θ = 418.23 mdeg), 518 nm (θ = −463.17 mdeg).

Chiral HPLC (ChiralPak IA, hexane/DCM/ethanol = 90/5/5, flow rate = 0.5 mL min^{-1}, λ = 450 nm, 25 °C): 28.10 min, ee = 96%.

$[Co_4SO_2TCA(\mu_4\text{-}OH_2)]_6[\Lambda\text{-}Co(L)_3]_8$. Yield = 74%.

ESI-MS: calculated *m*/*z* for $[M + H_2O - 6H]^{6-}$ 2226.3, *m*/*z* found 2227.5.

IM-MS: found $^{DT}CCS_{N_2}$ = 1830.0 Å^2.

Elemental analysis ($C_{624}H_{504}Co_{32}N_{48}O_{126}S_{24}\cdot 42DMF\cdot 23H_2O$): % calculated: C, 53.52%; H, 5.05%; N, 7.49%; % found: C, 53.54%; H, 4.95%; N, 7.49%.

CD (5×10^{-5} M, DCM, 2 mm): 467 nm (θ = −401.79 mdeg), 518 nm (θ = 433.51 mdeg).

Chiral HPLC (ChiralPak IA, hexane/DCM/ethanol = 90/5/5, flow rate = 0.5 mL min^{-1}, λ = 450 nm, 25 °C): 51.06 min, ee = 97%.

$[Ni_4SO_2TCA(\mu_4\text{-}OH_2)]_6[\Delta\text{-}Co(L)_3]_8$. Yield = 78%.

ESI-MS: calculated *m*/*z* for $[M + H_2O - 6H]^{6-}$ 2225.3, *m*/*z* found 2224.4.

IM-MS: found $^{DT}CCS_{N_2}$ = 1846.1 Å^2.

Elemental analysis ($C_{624}H_{504}Co_8Ni_{24}N_{48}O_{126}S_{24}\cdot 41DMF\cdot 34H_2O$): % calculated: C, 52.93%; H, 5.11%; N, 7.35%;% found: C, 52.92%; H, 5.08%; N, 7.36%.

CD (5×10^{-5} M, DCM, 2 mm): 464 nm (θ = 421.29 mdeg), 517 nm (θ = −479.56 mdeg).

Chiral HPLC (ChiralPak IA, hexane/DCM/ethanol = 90/5/5, flow rate = 0.5 mL min^{-1}, λ = 450 nm, 25 °C): 28.15 min, ee = 92%.

$[Ni_4SO_2TCA(\mu_4\text{-}OH_2)]_6[\Lambda\text{-}Co(L)_3]_8$. Yield = 53%.

ESI-MS: calculated *m*/*z* for $[M + H_2O - 6H]^{6-}$ *m*/*z* 2225.3 found *m*/*z* 2226.2.

IM-MS: found $^{DT}CCS_{N_2}$ = peak not resolved.

Elemental analysis ($C_{624}H_{504}Co_8Ni_{24}N_{48}O_{126}S_{24}\cdot 41DMF\cdot 31H_2O$): % calculated: C, 53.10%; H, 5.09%; N, 7.38%; % found: C, 53.09%; H. 5.07%; N. 7.39%.

CD (5×10^{-5} M, DCM, 2 mm): 464 nm (θ = −395.16 mdeg), 517 nm (θ = 452.06 mdeg).

Chiral HPLC (ChiralPak IA, hexane/DCM/ethanol = 90/5/5, flow rate = 0.5 mL min^{-1}, λ = 450 nm, 25 °C): 51.04 min, ee = 95%.

Characterization techniques

Elemental analysis was performed on a Vario Macro CHN analyzer (Elementar Analysen systeme GmbH, Langenselbold, Germany).

ESI-MS and ion mobility mass spectrometry. Ion mobility mass spectrometry experiments were performed with an Agilent 6560 ESI-IM-QTOF mass spectrometer equipped with a dual AJS ion source and a Drift Gas Upgrade Kit (Agilent Technologies, USA). Samples of **$[M_4SO_2TCA(\mu_4\text{-}kOH_2)]_6[\Delta,\Lambda\text{-}Co(L)_3]$** (M = Co or Ni) (0.005 g) were suspended in 250 µL of DCM and then filtered and the solution was diluted with 1 or 5 µL mL^{-1} ACN. All measurements were done using negative mode (−)ESI at an extended *m*/*z* range with N_2 and He as drift gases. The samples were injected into the ESI source with a flow rate of 5 µL min^{-1}. A dry gas temperature of 225 °C, a dry gas flow rate of 2 L min^{-1}, a nebulizer pressure of 5 psi, a sheath gas temperature of 225 °C, and a sheath gas flow rate of 5 L min^{-1} were used. A capillary voltage of 4000 V, a nozzle voltage of 2000 V and a fragmentor voltage of 400 V were set as source parameters. In the IM-MS experiments with N_2 drift gas (He values in parentheses), the drift tube pressure was set to 3.95 Torr and high-pressure funnel to 3.80 Torr (3.70 Torr). In the single-field IM experiments, the drift tube entrance and exit voltages were set as 1574 V (875 V) and 224 V (133 V), respectively. A trap filling time of 10 000 µs (5000 µs) and a trap release time of 150 µs (350 µs) were used. Collision cross-section (CCS) values were determined using multifield measurements and then the drift tube entrance voltage was varied from 1074 V to 1674 V with 100 V increments (563 to 875 V with 52 V increments). Before sample introduction, ES tuning mix (Agilent Technologies) was measured as a quality control sample for CCS values.[63] Data were analysed using MassHunter Qualitative Navigator (B.09.00) and MassHunter IM-MS Browser (B.08.00) from Agilent Technologies, USA.

Single crystal X-ray diffraction. Single crystal X-ray data were measured using a Rigaku SuperNova dual-source Oxford diffractometer equipped with an Atlas detector using mirror-monochromated Cu-Kα (λ = 1.54184 Å) radiation. Data collection and reduction were performed using the program CrysAlisPro,[64] with an empirical absorption correction method using spherical harmonics correction applied. The structure was solved with intrinsic phasing (ShelXT)[65] and refined by full-matrix least squares on F^2 using the Olex2 software,[66] which utilises the ShelXL-2015 module.[67] Anisotropic displacement parameters were assigned to non-H atoms. All hydrogen atoms were refined using riding models with U_{eq}(H) of $1.5U_{eq}$(C) for sp^3 hybridized carbons and U_{eq}(H) of $1.2U_{eq}$(C) for sp^2 hybridized carbons.†

Powder X-ray diffraction. Powder diffraction patterns were recorded in the Debye–Scherrer geometry using a PANalytical X'Pert PRO MPD diffractometer. Crystalline samples were ground and sealed in glass capillaries under a mother liquor.

Solvent vapor sorption. Solvent vapor sorption isotherms were measured at 298 K by a gravimetric dynamic vapor sorption method using a Surface Measurement Systems DVS resolution apparatus in the p/p_0 range from 0 to 90% in N_2 carrier gas. Freshly filtered off samples were placed in the DVS chamber and activated under a dry N_2 flow with a stepwise increase of temperature up to 393 K. All activation and measurement steps were carried out to achieve a stable mass of the samples (dm/dt = ±0.002% min^{-1}).

HPLC. HPLC measurements were realized on a Shimadzu Prominence HPLC system with a LC-20AD pump and SPD-M20A PDA detector. The data were analyzed using Labsolution software. The solvents used were of the HPLC Chromasolv grade quality.

($\Lambda/\Delta\text{-}Co(HL)_3$). 1 µL of the samples was injected into a Daicel Chiral column IA (4.6 mm × 250 mm; 5 µm). The chromatographic conditions were the following: a flow rate of 0.8 mL mn^{-1}, consisting of hexane/THF with 0.1% TFA at 80/20 and 25 °C. All samples passed through a PTFE filter (pore size: 0.2 µm) and were solubilized with hexane/THF at 50/50 as an injection mixture at a concentration of around 0.8 mg mL^{-1}.

$[M_4SO_2TCA(\mu_4\text{-}OH_2)]_6[\Lambda/\Delta\text{-}Co(L)_3]_8$ (M = Ni or Co). 1 µL of the samples was injected into a Daicel Chiral column IA (4.6 mm × 250 mm; 5 µm). The chromatographic conditions were the following: a flow rate of 0.5 mL min^{-1} with hexane/DCM/EtOH at 90/5/5 as the eluent mixture at 25 °C. All samples passed through a PTFE filter (pore size: 0.2 µm) and were solubilized with DCM/EtOH at 86/14 as the injection mixture at a concentration of around 0.5 mg mL^{-1}.

Conclusions

We reported a reliable approach for the synthesis of chiral porous octahedral nanosized coordination cages, resulting from the three-component assembly of sulfonylcalixarene, an enantiomerically enriched tris-dipyrrin complex and metallic cations. Two pairs of enantiomers were obtained and, to the best of our knowledge, this is the first example of calixarene-based MOCs, where a metallic stereogenic center is used, which leads to face-induced chirality of the nanosized objects. This paves the way to a new class of materials. The obtained supramolecular architectures, which incorporate 32 metal cations and display large cavities (*ca.* 19 Å), exhibit internal and external porosity. The porosity was illustrated through DVS measurements, and the compounds display high water affinity (intake of up to 80 molecules). The sorption of 2-butanol was also revealed to be high (up to 76 molecules) without any enantioselectivity towards enantiopure *S*-2-butanol. The enantioselectivity towards larger species and the reactivity of these species as enantioselective catalysts are currently under investigation.

Author contributions

Ivan V. Khariushin: formal analysis, investigation, writing, reviewing and conceptualization. Alexander S. Ovsyannikov: formal analysis, methodology conceptualization, reviewing and supervision. Stéphane A. Baudron: conceptualization and reviewing. Jas S. Ward: investigation, data curation and reviewing. Anniina Kiesila: investigation and data curation. Kari Rissanen: investigation and data curation. Elina Kalenius: investigation and data curation. Matthieu Chessé: investigation and data curation. Beata Nowicka: investigation and data curation. Svetlana E. Solovieva: funding administration. Igor S. Antipin: funding administration. Véronique Bulach: methodology, funding, reviewing and supervision. Sylvie Ferlay: methodology, funding, writing, reviewing, editing and supervision.

Data availability

The data supporting this article have been included as part of the ESI.†

Conflicts of interest

There are no conflicts to declare.

Acknowledgements

This work was supported by the University of Strasbourg, Fondation Jean-Marie Lehn, Doctoral Verdnaskii scholarship from the French Embassy (I. V. K.), the CNRS and the Russian Science Foundation (Project No. 19-73-20035 to A. S. O., S. E. S. and I. S. A.). The University of Jyväskylä is acknowledged for the use of SCXRD and MS instrumentation.

References

1 S. J. Dalgarno, N. P. Power and J. L. Atwood, Metallo-Supramolecular Capsules, *Coord. Chem. Rev.*, 2008, **252**, 825–841.

2 H. Li, Z.-J. Yao, D. Liu and G.-X. Jin, Multi-Component Coordination-Driven Self-Assembly Toward Heterometallic Macro- cycles and Cages, *Coord. Chem. Rev.*, 2015, **293**, 139–157.

3 T. R. Cook and P. J. Stang, Recent Developments in the Preparation and Chemistry of Metallacycles and Metallacages via Coordination, *Chem. Rev.*, 2015, **115**, 7001–7045.

4 N. Hosono and S. Kitagaw, Modular Design of Porous Soft Materials via Self-Organization of Metal-Organic Cages, *Acc. Chem. Res.*, 2018, **51**, 2437–2446.

5 E.-S. M. El-Sayed and D. Yuan, Metal-Organic Cages (MOCs): From Discrete to Cage-based Extended Architectures, *Chem. Lett.*, 2020, **49**, 28–53.

6 S. Lee, H. Jeong, D. Nam, M. S. Lah and W. Choe, The rise of metal-organic polyhedra, *Chem. Soc. Rev.*, 2021, **50**, 528–555.

7 M. J. Bojdys, M. E. Briggs, J. T. A. Jones, D. J. Adams, S. Y. Chong, M. Schmidtmann and A. I. Cooper, Supramolecular Engineering of Intrinsic and Extrinsic Porosity in Covalent Organic Cages, *J. Am. Chem. Soc.*, 2011, **133**, 16566–16571.

8 I. A. Riddell, M. M. J. Smulders, J. K. Clegg and J. R. Nitschke, Encapsulation, Storage and Controlled Release of Sulfur Hexafluoride from a Metal-Organic Capsule, *Chem. Commun.*, 2011, **47**, 457–459.

9 A. C. Sudik, A. R. Millward, N. W. Ockwig, A. P. Côté, J. Kim and O. M. Yaghi, Design, Synthesis, Structure, and Gas (N_2, Ar, CO_2, CH_4, and H_2) Sorption Properties of Porous Metal-Organic Tetrahedral and Heterocuboidal Polyhedra, *J. Am. Chem. Soc.*, 2005, **127**, 7110–7118.

10 S. Furukawa, N. Horike, M. Kondo, Y. Hijikata, A. Carné-Sanchez, P. Larpent, N. Louvain, S. Diring, H. Sato, R. Matsuda, R. Kawano and S. Kitagawa, Rhodium-Organic Cuboctahedra as Porous Solids with Strong Binding Sites, *Inorg. Chem.*, 2016, **55**, 10843–10846.

11 A. Brzechwa-Chodzyńska, W. Drożdż, J. Harrowfield and A. R. Stefankiewicz, Fluorescent sensors: A bright future for cages, *Coord. Chem. Rev.*, 2021, **434**, 213820.

12 C. J. Brown, F. D. Toste, R. G. Bergman and K. N. Raymond, Supramolecular Catalysis in Metal-Ligand Cluster Hosts, *Chem. Rev.*, 2015, **115**, 3012–3035.

13 W. Cullen, M. C. Misuraca, C. A. Hunter, N. H. Williams and M. D. Ward, Highly efficient catalysis of the Kemp elimination in the cavity of a cubic coordination cage, *Nat. Chem.*, 2016, **8**, 231–236.

14 E. G. Percástegui, T. K. Ronson and J. R. Nitschke, Design and Applications of Water-Soluble Coordination Cages, *Chem. Rev.*, 2020, **120**(24), 13480–13544.

15 J.-S. M. Lee, K.-I. Otake and S. Kitagawa, Transport properties in porous coordination polymers, *Coord. Chem. Rev.*, 2020, **421**, 213447–213457.

16 H. Sepehrpour, W. Fu, Y. Sun and P. J. Stang, Biomedically Relevant Self-Assembled Metallacycles and Metallacages, *J. Am. Chem. Soc.*, 2019, **141**, 14005–14020.

17 Y.-P. Wang, Y. Zhang, X.-H. Duan, J.-J. Mao, M. Pan, J. Shen and C.-Y. Su, Recent progress in metal-organic cages for biomedical application: Highlighted research during 2018-2023, *Coord. Chem. Rev.*, 2024, **501**, 215570.

18 P. Mal, B. Breiner, K. Rissanen and J. R. Nitschke, White phosphorus is air-stable within a self-assembled tetrahedral capsule, *Science*, 2009, **324**, 1697–1699.

19 D. Fujita, Y. Ueda, S. Sato, H. Yokoyama, N. Mizuno, T. Kumasaka and M. Fujita, Self-Assembly of $M_{30}L_{60}$ Icosidodecahedron, *Chem*, 2016, **1**, 91–101.

20 H. Kumagai, M. Hasegawa, S. Miyanari, Y. Sugawa, Y. Sato, T. Hori, S. Ueda, H. Kamiyama and S. Miyano, Facile synthesis of p-tert-butylthiacalix[4]arene by the reaction of p-tert-butylphenol with elemental sulfur in the presence of a base, *Tetrahedron Lett.*, 1997, **38**, 3971–3974.

21 G. Mislin, E. Graf, M. W. Hosseini and A. De Cian, Sulfonecalixarenes: a new class of molecular building block, *J. Chem. Soc., Chem. Commun.*, 1998, 1345–1346.

22 C. D. Gutsche, *Calixarenes Revised: Monographs in Supramolecular Chemistry*, The Royal Society of Chemistry, Cambridge, 1998, vol. 6.

23 A. Ikeda and S. Shinkai, Novel Cavity Design Using Calix[n] arene Skeletons: Toward Molecular Recognition and Metal Binding, *Chem. Rev.*, 1997, **97**, 1713–1734.

24 J. L. Atwood, L. J. Barbour and A. Jerga, Storage of Methane and Freon by Interstitial van der Waals Confinement, *Science*, 2002, **296**, 2367–2369.

25 N. Morohashi and T. Hattori, Selective guest inclusion by crystals of calixarenes: potential for application as separation materials, *J. Inclusion Phenom. Macrocyclic Chem.*, 2018, **90**, 261–277.

26 M. A. Sinnwell, J. L. Atwood and P. K. Thallapally, Sorption of CO_2 in a hydrogen-bonded diamondoid network of sulfonylcalix[4]arene, *Supramol. Chem.*, 2018, **30**, 540–544.

27 M. Liu, W. Liao, C. Hu, S. Du and H. Zhang, Calixarene-Based Nanoscale coordination Cages, *Angew. Chem., Int. Ed.*, 2012, **51**, 1585–1588.

28 Y. Bi, S. Du and W. Liao, Thiacalixarene-based nanoscale polyhedral coordination cages, *Coord. Chem. Rev.*, 2014, **276**, 61–72.

29 Q.-W. Zeng, L. Hu, Y. Niu, D. Wang, Y. Kang, H. Jia, W.-T. Dou and L. Xu, Metal–organic cages for gas adsorption and separation, *Chem. Commun.*, 2024, **60**, 3469–3483.

30 N. Iki, H. Kumagai, N. Morohashi, K. Ejima, M. Hasegawa, S. Miyanari and S. Miyano, Selective oxidation of thiacalix[4]arenes to the sulfinyl- and sulfonylcalix[4]arenes and their coordination ability to metal ions, *Tetrahedron Lett.*, 1998, **39**, 7559–7562.

31 F.-R. Dai, U. Sambasivam, A. J. Hammerstrom and Z. Wang, Synthetic Supercontainers Exhibit Distinct Solution versus Solid State Guest-Binding Behavior, *J. Am. Chem. Soc.*, 2014, **136**, 7480–7491.

32 N. L. Netzer, F.-R. Dai, Z. Wang and C. Jiang, pH-Modulated Molecular Assemblies and Surface Properties of Metal–Organic Supercontainers at the Air–Water Interface, *Angew. Chem., Int. Ed.*, 2014, **53**, 10965–10969.

33 K. Xiong, F. Jiang, Y. Gai, D. Yuan, L. Chen, M. Wu, K. Su and M. Hong, Truncated octahedral coordination cage incorporating six tetranuclear-metal building blocks and twelve linear edges, *Chem. Sci.*, 2012, **1**, 2321–2325.

34 I. V. Khariushin, V. Bulach, S. Solovieva, I. Antipin, A. Ovsyannikov and S. Ferlay, Thiacalix[4]arene macrocycles as versatile building blocks for the rational design of high-nuclearity metallic clusters, metallamacrocycles, porous coordination cages and containers, *Coord. Chem. Rev.*, 2024, **513**, 215846.

35 T. Kajiwara, T. Kobashi, R. Shinagawa, T. Ito, S. Takaishi, M. Yamashita and N. Iki, Highly Symmetrical Tetranuclear Cluster Complexes Supported by p-tert- Butylsulfonylcalix[4]arene as a Cluster-Forming Ligand, *Eur. J. Inorg. Chem.*, 2006, 1765–1770.

36 W. Gong, D. D. Chu, H. Jiang, X. Chen, Y. Cui and Y. Liu, Permanent porous hydrogen-bonded frameworks with two types of brønsted acid sites for heterogeneousasymmetric catalysis, *Nat. Commun.*, 2019, **10**, 600.

37 M. V. Kniazeva, A. S. Ovsyannikov, A. I. Samigullina, D. R. Islamov, A. T. Gubaidullin, P. V. Dorovatovskii, V. A. Lazarenko, S. E. Solovieva, I. S. Antipin and S. Ferlay, Impact of flexible succinate connectors on the formation of tetrasulfonylcalix[4]arene based nano-sized polynuclear cages: structural diversity and induced chirality study, *CrystEngComm*, 2022, **24**, 628–638.

38 C. Tan, J. Jiao, Z. Li, Y. Liu, X. Han and Y. Cui, Design and Assembly of a Chiral Metallosalen-Based Octahedral Coordination Cage for Supramolecular Asymmetric Catalysis, *Angew. Chem., Int. Ed.*, 2018, **57**, 2085–2090.

39 M. Pan, K. Wu, J.-H. Zhang and C.-Y. Su, Chiral metal–organic cages/containers (MOCs): From structural and stereochemical design to applications, *Coord. Chem. Rev.*, 2019, **378**, 333–349.

40 L. Zhang, H. Liu, G. Yuan and Y.-F. Han, Chiral Coordination Metallacycles/Metallacages for Enantioselective Recognition and Separation, *Chin. J. Chem.*, 2021, **39**, 2273–2286.

41 E. Yashima, K. Maeda and Y. Okamoto, Memory of macromolecular helicity assisted by interaction with achiral small molecules, *Nature*, 1999, **399**, 449–451.

42 W. Meng, K. K. Clegg, J. D. Thoburn and J. R. Nitschke, Controlling the Transmission of Stereochemical Information through Space in Terphenyl-Edged Fe_4L_6 Cages, *J. Am. Chem. Soc.*, 2011, **133**, 13652–13660.

43 J. Dong, C. Tan, K. Zhang, Y. Liu, P. J. Low, J. Jiang and Y. Cui, Chiral NH-Controlled Supramolecular Metallacycles, *J. Am. Chem. Soc.*, 2017, **139**, 1554–1564.

44 J. Guo, Y.-W. Xu, K. Li, L.-M. Xiao, S. Chen, K. Wu, X.-D. Chen, Y.-Z. Fan, J.-M. Liu and C.-Y. Su, Regio- and Enantioselective Photodimerization within the Confined

Space of a Homochiral Ruthenium/Palladium Heterometallic Coordination Cage, *Angew. Chem., Int. Ed.*, 2017, **56**, 3852–3856.

45 J. Jiao, C. Tan, Z. Li, Y. Liu, X. Han and Y. Cui, Design and Assembly of Chiral Coordination Cages for Asymmetric Sequential Reactions, *J. Am. Chem. Soc.*, 2018, **140**, 2251–2259.

46 I. V. Khariushin, A. S. Ovsyannikov, S. A. Baudron, J. S. Ward, A. Kiesilä, K. Rissanen, E. Kalenius, K. A. Kovalenko, V. P. Fedin, S. E. Solovieva, I. S. Antipin, V. Bulach and S. Ferlay, Selective gas adsorption by calixarene-based porous octahedral M_{32} coordination cages, *Chem. Commun.*, 2022, **58**, 13628–13631.

47 K. Wu, K. Li, Y.-J. Hou, M. Pan, L.-Y. Zhang, L. Chen and C.-Y. Su, Homochiral D_4-symmetric metal–organic cages from stereogenic Ru(II) metalloligands for effective enantioseparation of atropisomeric molecules, *Nat. Commun.*, 2016, **7**, 10487.

48 J. Guo, Y.-W. Xu, K. Li, L.-M. Xiao, S. Chen, K. Wu, X.-D. Chen, Y.-Z. Fan, J.-M. Liu and C.-Y. Su, Regio- and Enantioselective Photodimerization within the Confined Space of a Homochiral Ruthenium/Palladium Heterometallic Coordination Cage, *Angew. Chem., Int. Ed.*, 2017, **56**, 3852–3856.

49 S. G. Telfer and J. D. Wuest, Metallotectons: using enantiopure tris(dipyrrinato)cobalt(III) complexes to build chiral molecular materials, *Chem. Commun.*, 2007, 3166–3168.

50 A. L. Spek, PLATON SQUEEZE: a tool for the calculation of the disordered solvent contribution to the calculated structure factors, *Acta Crystallogr., Sect. C:Struct. Chem.*, 2015, **71**, 9–18.

51 E. J. Gosselin, C. A. Rowland and E. D. Bloch, Permanently Microporous Metal–Organic Polyhedra, *Chem. Rev.*, 2020, **120**, 8987–9014.

52 Z.-K. Zhu, Y.-Y. Lin, H. Yu, X.-X. Li and S.-T. Zheng, Inorganic–Organic Hybrid Polyoxoniobates: Polyoxoniobate Metal Complex Cage and Cage Framework, *Angew. Chem., Int. Ed.*, 2019, **58**, 16864–16868.

53 J. Lianglu, W. Hu, X. Zhu, H.-Y. Zhang, L. Shi, X.-Q. Hao and M.-P. Song, Synthesis of a Tetrahedral Metal–Organic Supramolecular Cage with Dendritic Carbazole Arms, *Int. J. Mol. Sci.*, 2022, **23**, 15580.

54 W. Li, L. Sun, C. Liu, A. Rotaru, K. Robeyns, M. L. Singleton and Y. Garcia, Supramolecular $FeII_4L_4$ cage for fast ammonia sensing, *J. Mater. Chem. C*, 2022, **10**, 9216–9221.

55 G. R. Lorzing, A. J. Gosselin, B. A. Trump, A. H. P. York, A. Sturluson, C. A. Rowland, G. P. A. Yap, C. M. Brown, C. M. Simon and E. D. Bloch, Understanding Gas Storage in Cuboctahedral Porous Coordination Cages, *J. Am. Chem. Soc.*, 2019, **141**, 12128–12138.

56 K. Jin, D. Moon, M. Kim and J. Park, Tailoring the extrinsic porosity of a vapochromic metal-organic polyhedron for rapid VOC detection, *Sens. Actuators, B*, 2023, **393**, 134205.

57 R.-G. Xiong, X.-Z. You, B. F. Abrahams, Z. Xue and C.-M. Che, Enantioseparation of Racemic Organic Molecules by a Zeolite Analogue, *Angew. Chem., Int. Ed.*, 2001, **40**, 4422–4425.

58 Y. A. Satska, E. A. Mikhalyova, Z. V. Chernenko, S. V. Kolotilov, M. Zeller, I. V. Komarov, A. V. Tymtsunik, A. Tolmachev, K. S. Gavrilenko and A. W. Addison, Sorption discrimination between secondary alcohol enantiomers by chiral alkyl-dicarboxylate MOFs, *RSC Adv.*, 2016, **6**, 93707–93714.

59 Y. A. Satska, N. P. Komarova, K. S. Gavrilenko, O. V. Manoylenko, Z. V. Chernenko, M. A. Kiskin, S. V. Kolotilov, I. L. Eremenko and V. M. Novotortsev, Sorption and, separation of optical isomers of 2-butanol by chiral porous coordination polymers, *Theor. Exp. Chem.*, 2015, **51**, 45–53.

60 C.-M. Liu, D.-Q. Zhang, X. Hao and D.-B. Zhu, Syntheses, Crystal Structures, and Magnetic Properties of Two p-tert-Butylsulfonylcalix[4]arene Supported Cluster Complexes with a Totally Disordered $Ln_4(OH)_4$ Cubane Core, *Cryst. Growth Des.*, 2012, **12**, 2948–2954.

61 C. Brückner, Y. Zhang, S. J. Rettigand and D. Dolphin, Synthesis, derivatization and structural characterization of octahedral tris(5-phenyl-4,6-dipyrrinato) complexes of cobalt(Ill) and iron(Ill), *Inorg. Chim. Acta*, 1997, **263**, 279–286.

62 S. J. Garibay, J. R. Stork, Z. Wang, S. M. Cohen and S. G. Telfer, Enantiopure *vs.* racemic metalloligands: impact on metal–organic framework structure and synthesis, *Chem. Commun.*, 2007, 4881–4883.

63 (*a*) V. Gabelica, A. A. Shvartsburg, C. Afonso, P. Barran, J. L. P. Benesch, C. Bleiholder, M. T. Bowers, A. Bilbao, M. F. Bush, J. L. Campbell, I. D. G. Campuzano, T. Causon, B. H. Clowers, C. S. Creaser, E. De Pauw, J. Far, F. Fernandez-Lima, J. C. Fjeldsted, K. Giles, M. Groessl, C. J. Hogan, S. Hann, H. I. Kim, R. Kurulugama, J. C. May, J. A. McLean, K. Pagel, K. Richardson, M. E. Ridgeway, F. Rosu, F. Sobott, K. Thalassinos, S. J. Valentine and T. Wyttenbach, Recommendations for Reporting Ion Mobility Mass Spectrometry Measurements, *Mass Spectrom. Rev.*, 2019, **38**, 291–320; (*b*) S. M. Stow, T. J. Causon, X. Zheng, R. T. Kurulugama, T. Mairinger, J. C. May, E. E. Rennie, E. S. Baker, R. D. Smith and J. A. McLean, An Interlaboratory Evaluation of Drift Tube Ion Mobility–mass Spectrometry Collision Cross Section Measurements, *Anal. Chem.*, 2017, **89**, 9048–9055.

64 Rigaku Oxford Diffraction, *CrysAlisPro*, Rigaku Corporation, Oxford, UK, 2018.

65 G. M. Sheldrick, *SHELXT* - Integrated space-group and crystal-structure determination, *Acta Crystallogr., Sect. A: Found. Adv.*, 2015, **71**, 3–8.

66 O. V. Dolomanov, L. J. Bourhis, R. J. Gildea, J. A. K. Howard and H. Puschmann, OLEX2: a complete structure solution, refinement and analysis program, *J. Appl. Crystallogr.*, 2009, **42**, 339–341.

67 G. M. Sheldrick, Crystal structure refinement with SHELXL, *Acta Crystallogr., Sect. C:Struct. Chem.*, 2015, **71**, 3–8.